Eur. Phys. J. A **23**, 271–278 (2005)
DOI 10.1140/epja/i2004-10075-y

THE EUROPEAN PHYSICAL JOURNAL A

# Two-proton small-angle correlations in central heavy-ion collisions: A beam-energy– and system-size–dependent study

The FOPI Collaboration

R. Kotte[5,a], J.P. Alard[3], A. Andronic[1,4], V. Barret[3], Z. Basrak[12], N. Bastid[3], M.L. Benabderrahmane[6], R. Čaplar[12], E. Cordier[6], P. Crochet[3], P. Dupieux[3], M. Dželalija[12], Z. Fodor[2], I. Gašparić[12], A. Gobbi[4], Y. Grishkin[7], O.N. Hartmann[4], N. Herrmann[6], K.D. Hildenbrand[4], B. Hong[9], J. Kecskemeti[2], Y.J. Kim[9], M. Kirejczyk[6,11], P. Koczon[4], M. Korolija[12], T. Kress[4], A. Lebedev[7], Y. Leifels[6], X. Lopez[3], M. Merschmeyer[6], J. Mösner[5], W. Neubert[5], D. Pelte[6], M. Petrovici[1], F. Rami[10], W. Reisdorf[4], B. de Schauenburg[10], A. Schüttauf[4], Z. Seres[2], B. Sikora[11], K.S. Sim[9], V. Simion[1], K. Siwek-Wilczyńska[11], V. Smolyankin[7], G. Stoicea[1], Z. Tyminski[4,11], P. Wagner[10], K. Wiśniewski[11], D. Wohlfarth[5], Z.G. Xiao[4], Y. Yushmanov[8], and A. Zhilin[7]

[1] Institute for Nuclear Physics and Engineering, Bucharest, Romania
[2] Central Research Institute for Physics, Budapest, Hungary
[3] Laboratoire de Physique Corpusculaire, IN2P3/CNRS and Université Blaise Pascal, Clermont-Ferrand, France
[4] Gesellschaft für Schwerionenforschung, Darmstadt, Germany
[5] IKH, Forschungszentrum Rossendorf, PF 510119, D-01314 Dresden, Germany
[6] Physikalisches Institut der Universität Heidelberg, Heidelberg, Germany
[7] Institute for Theoretical and Experimental Physics, Moscow, Russia
[8] Kurchatov Institute for Atomic Energy, Moscow, Russia
[9] Korea University, Seoul, Korea
[10] Institut de Recherches Subatomiques, IN2P3-CNRS/ULP, Strasbourg, France
[11] Institute of Experimental Physics, Warsaw University, Warsaw, Poland
[12] Rudjer Bošković Institute Zagreb, Zagreb, Croatia

Received: 17 May 2004 / Revised version: 24 August 2004 /
Published online: 19 November 2004 – 
Communicated by W. Henning

**Abstract.** Small-angle correlations of pairs of protons emitted in central collisions of Ca + Ca, Ru + Ru and Au + Au at beam energies from 400 to 1500 MeV per nucleon are investigated with the FOPI detector system at SIS/GSI Darmstadt. Dependences on system size and beam energy are presented which extend the experimental data basis of pp correlations in the SIS energy range substantially. The size of the proton-emitting source is estimated by comparing the experimental data with the output of a final-state interaction model which utilizes either static Gaussian sources or the one-body phase-space distribution of protons provided by the BUU transport approach. The trends in the experimental data, *i.e.* system size and beam energy dependences, are well reproduced by this hybrid model. However, the pp correlation function is found rather insensitive to the stiffness of the equation of state entering the transport model calculations.

**PACS.** 25.70.Pq Multifragment emission and correlations – 25.75.Gz Particle correlations

## 1 Introduction

Two-proton correlation functions at small relative momenta can probe the space-time extent of the reaction zone created in energetic heavy-ion reactions. This is due to the fact that the magnitude of nuclear and Coulomb final-state interactions (FSI) as well as antisymmetrization effects depend on the spatial separation of the two protons during the emission process [1–22]. Usually, the correlation functions are evaluated as a function of the magnitude $q$ of the relative momentum vector $\mathbf{q} = (\mathbf{p}_1 - \mathbf{p}_2)/2$. The interplay of the attractive $S$-wave nuclear interaction and the Coulomb repulsion and antisymmetrization produce a minimum at $q = 0$ and a maximum in the correlation function at $q \sim 20$ MeV/$c$ [1]. Most analyses give only upper limits for the spatial extent of the source due to the ambiguity of radius and lifetime of the source, *i.e.* model calculations simulating large sources with short lifetimes will give very similar correlation functions as model calculations simulating small sources with long lifetimes [1,5].

[a] e-mail: kotte@fz-rossendorf.de

At beam energies below about 100 $A \cdot$MeV, heavy-ion experiments performed mainly at the National Superconducting Cyclotron Laboratory (NSCL) at Michigan State University (MSU) [3,5,11–17] allowed for systematic investigations of pp small-angle correlations. Furthermore, new methods allowing to deduce the emission source function from two-particle correlations have been proposed. Thus, recently, the technique of source imaging [23–26], *i.e.* the numerical inversion of the correlation function, has been applied successfully to pp correlations studied in heavy-ion experiments not only in the MSU-NSCL energy range [23,27,28] but also at significantly higher beam energies provided by the Brookhaven-AGS [29] or even by the CERN-SPS [30].

However, in the energy domain of the heavy-ion synchrotron SIS at GSI Darmstadt, ranging from about 100 to 2000 $A\cdot$MeV, only few data on pp correlations are available: proton-proton correlations at small relative momenta were measured with the "Plastic Ball" at BEVALAC for two systems, Ca on Ca and Nb on Nb, at 400 $A \cdot$ MeV as a function of proton multiplicity [9]. Freeze-out densities of about 25% of normal nuclear-matter density were extracted. Two-proton small-angle correlations were studied at SATURNE in Ar + Au reactions at 200 $A \cdot$ MeV [10] and in Ne- and Ar-nucleus collisions between 200 and 1000 $A \cdot$ MeV [4]. Breakup densities and time scales in spectator fragmentation following the reaction Au + Au at 1 $A \cdot$ GeV were investigated with the ALADiN spectrometer at SIS/GSI [18,19]. Finally, the space-time extent of the proton-emitting source was studied with the $4\pi$ detector FOPI measuring central collisions of Ni + Ni at 1930 $A\cdot$MeV and of Ru + Ru at 400 $A\cdot$MeV [20,22]. Consequently, the extension of the pp-correlation data base is highly desirable.

Since the theoretical pp correlation function only requires the knowledge of the one-body phase-space distribution of protons, it is possible to generate small-angle correlations with any microscopic theory that calculates the time evolution of the one-body distribution function [7]. In addition to the usage of Gaussian source distributions we will also follow this procedure since it allows a more adequate comparison of experimental and theoretical correlation functions. Microscopic transport models, like Boltzmann-Uehling-Uhlenbeck (BUU) [6–8] or Quantum Molecular Dynamics (QMD) [31] in their various implementations, do not only allow to trace the expectation values of the positions of the various particles in coordinate space but also the corresponding time information. Moreover, they carry the correlation of coordinate and momentum space coordinates of the individual particles. This correlation is generated intrinsically during the expansion following the compression phase of the heavy-ion collision. On a macroscopic scale, the expansion constitutes a collective motion of the various particle species, called radial flow. Thus, it is natural to expect that a hybrid model consisting of BUU approach plus FSI model should be able to reproduce the experimental data and give the relevant insight into the physics of the heavy-ion collision until particle freeze out. Furthermore, there is reasonable hope that a systematic comparison of as much as possible experimental information, *e.g.* on sideward [32] and elliptic flow [33], on nuclear stopping [34] and cluster production [35], on the shape (in momentum space) of the participant source [36] or on charged pion production [37], with transport model predictions will allow to constrain the essential input parameters of the model, *e.g.* the equation of state (EoS) and/or the nucleon-nucleon cross-section within the nuclear medium. Earlier it was reported that the pp correlation function generated for $^{14}$N + $^{27}$Al collisions at 75 $A\cdot$MeV is only weakly dependent on the EoS [5,8]. It is not clear whether the sensitivity to the microscopic details of the transport approach increases for higher beam energies and/or heavier projectile-target combinations. Therefore, in the following we will study in a systematic way how the BUU+FSI hybrid model reproduces the data and what kind of information can be gained.

The paper is structured as follows: In sect. 2 the experimental basis is described shortly, the involved event classes are explained and the correlation function is defined. In sect. 3 the experimental pp correlation functions with their dependences on system size and beam energy are presented and compared to model predictions. Finally, the results are summarized in sect. 4.

## 2 The experiment

The experiments have been performed at the heavy-ion synchrotron SIS at GSI Darmstadt. Symmetric collisions are carried out by irradiating targets of 1% interaction thickness of $^{40}$Ca and $^{197}$Au with the corresponding ions of beam energies between 400 and 1500 $A \cdot$ MeV. At a projectile energy of 400 $A \cdot$ MeV the system of intermediate mass, $^{96}$Ru + $^{96}$Ru, is included which was explored extensively with respect to the space-time difference of light-charged particles emission in central collisions [22].

The present analysis uses a subsample of the data, taken with the outer Plastic Wall/Helitron combination of the FOPI detector system [38,39]. The Plastic Wall delivers —via energy loss *vs.* time-of-flight (TOF) measurement— the nuclear charge $Z$ and the velocity $\beta$ of the produced particles and the corresponding hit positions. The Helitron gives the curvature (which is a measure of momentum over charge $(p/Z)$) of the particle track in the field of a large superconducting solenoid. Since the momentum resolution of the Helitron is rather moderate, this detector component serves for particle identification only. The mass $m$ is determined via $mc = (p/Z)_{\mathrm{Hel}}/(\beta\gamma/Z)_{\mathrm{Pla}}$, where $\gamma = (1-\beta^2)^{-1/2}$. The Plastic Wall and the Helitron have full overlap only for polar angles between 8.5 degrees and 26.5 degrees. The corresponding flight paths amount to 450 cm and 380 cm, respectively. Monte Carlo simulations have been performed in order to study the influence of the finite detector granularity and of the TOF and position resolutions on the velocity and finally on the proton momentum. The resolution of both quantities is governed by the TOF resolution, which is $\sigma_{\mathrm{TOF}} = 80$ (120) ps for short (long) scintillator strips located at small (large) polar angles [38]. The velocity can be determined with a precision of $\delta\beta/\beta < 1\%$.

### 2.1 Event classification

Typically, a few hundred thousand to a million central events are collected for each individual collision system by demanding large charged-particle multiplicities to be measured in the outer Plastic Wall. The corresponding integrated cross-sections for the collision systems Ca + Ca, Ru + Ru, and Au + Au comprise about 15%, 10% and 10% of the total cross-section, respectively. For the present central-event class one would expect —within a geometrical picture— average impact parameters of about 2 fm, 2 fm, and 3 fm. Taking into account typical dispersions of the impact parameter distribution of about 1 fm as found from GEANT simulations [40], the number of participants in the central source is estimated to $A_{\rm part} = 56 \pm 12$ ($147 \pm 21$, $302 \pm 34$) for the system Ca + Ca (Ru + Ru, Au + Au). More peripheral collisions have been measured, too. But, due to both the strong downscaling (typically a factor of 16) of the corresponding online trigger and the lower proton multiplicities, the pp pair statistics was not sufficient for correlation analyses.

In previous investigations of central Au + Au collisions between 100 and 400 $A \cdot$ MeV beam energy it was found that the correlation function of pairs of intermediate mass fragments is strongly affected by the collective directed sideward flow of nuclear matter [41,42]. This directed sideflow causes an enhancement of correlations at small relative momenta. The enhancement results from mixing of differently azimuthally oriented events; it vanishes if the events are rotated into a unique reaction plane, which is determined by the standard transverse momentum analysis [43]. Consequently, the technique of event rotation is applied also to the present data in order to prevent such artificial correlations from being introduced into the reference momentum distribution of the correlation function (cf. sect. 2.2).

### 2.2 Correlation function

Let $Y_{12}(\mathbf{p}_1, \mathbf{p}_2)$ be the coincidence yield of pairs of particles having momenta $\mathbf{p}_1$ and $\mathbf{p}_2$. Then the two-particle correlation function is defined as

$$1 + R(\mathbf{p}_1, \mathbf{p}_2) = \mathcal{N} \frac{\sum_{\rm events,pairs} Y_{12}(\mathbf{p}_1, \mathbf{p}_2)}{\sum_{\rm events,pairs} Y_{12,\rm mix}(\mathbf{p}_1, \mathbf{p}_2)} \,. \quad (1)$$

The sum runs over all events fulfilling the abovementioned global selection criterion and over all pairs satisfying certain conditions given below. Event mixing, denoted by the subscript "mix", means to take particle 1 and particle 2 from different events. The normalization factor $\mathcal{N}$ is fixed by the requirement to have the same number of true and mixed pairs. The statistical errors of all the correlation functions presented below are governed by those of the coincidence yield, since the mixed yield is generated with two orders of magnitude higher statistics. The correlation function (1) is then projected onto the relative momentum

$$q = |\mathbf{q}| = \frac{1}{2} |\mathbf{p}_1^{\rm cm} - \mathbf{p}_2^{\rm cm}|. \quad (2)$$

Here, $\mathbf{p}_i^{\rm cm}$ are the particle momenta calculated in the c.m. system of the colliding nuclei. From the velocity resolution as estimated in sect. 2, the corresponding $q$ resolution is deduced to be $\delta q = (4 \pm 1)$ MeV/$c$. A similar value can be derived directly from the experimental dispersion of the resonance due to the narrow 2.186 MeV state of $^6$Li ($J^\pi = 3^+$, $\Gamma = 24$ keV) in the $\alpha$-d correlation function [22]. All theoretical correlation functions presented in sect. 3 are folded with this $q$ resolution.

As in previous proton-proton correlation analyses [20–22] an enhanced coincidence yield at very small relative angles is observed, which is due to double counting caused mainly by scattering in the scintillator strips. This disturbing yield is reduced strongly by the requirement to match the particle hits on the Plastic Wall with the corresponding tracks in the forward drift chamber Helitron. The remaining left-over of doubly counted scattered particles is eliminated by excluding, around a given hit, positions within a rectangular segment of azimuthal and polar angle differences $|\phi_1 - \phi_2| < 4^\circ$ and $|\theta_1 - \theta_2| < 2^\circ$. The same procedure is applied to the uncorrelated background, hence keeping the influence of the exclusion onto the correlation function as small as possible. GEANT simulations [40] have shown that at very small relative momenta, $q <$ (12–15) MeV/$c$, still a small bias of the correlation function can not be excluded [20,22]. Thus, the corresponding regions in the correlation functions are not taken into consideration when comparing the experimental data with model predictions.

## 3 Results and comparison with model predictions

For description of the FSI model we refer to ref. [22] and references cited therein. As source distributions we use either Gaussian density profiles in coordinate and momentum space or the output of the BUU transport model. The theoretical correlation function is given as

$$1 + R(\mathbf{P}, \mathbf{q}) = \int {\rm d}^3 r \, S(\mathbf{r}, \mathbf{P}) \, |\Psi_{\mathbf{q}}(\mathbf{r})|^2. \quad (3)$$

Here, the wave function $\Psi$ describes the relative motion of the two emitted particles and $S$ is the source function. Gaussian sources are defined in [22]. In case of calculating the single-particle phase-space distribution within the BUU model, the source function is given as

$$S(\mathbf{r}, \mathbf{P}) = \mathcal{N}_p \sum_{i,j} \delta\left(\frac{\mathbf{P}}{2} - \mathbf{p}_i\right) \delta\left(\frac{\mathbf{P}}{2} - \mathbf{p}_j\right) \times \delta\left(\mathbf{r} - (\mathbf{r}_i - \mathbf{r}_j) + \frac{\mathbf{P}}{2m}(t_i - t_j)\right). \quad (4)$$

$\mathbf{r}_i$, $t_i$, and $\mathbf{p}_i$ are the space, time and momentum coordinates of particle $i$ at freeze out. The parameter $\mathbf{P}$ represents the sum momentum of the observed particle pair. The normalization $\mathcal{N}_p$ is chosen such that

$$\int {\rm d}^3 r \, S(\mathbf{r}, \mathbf{P}) = 1. \quad (5)$$

To allow the summation over a sufficient number of particles, the $\delta$ function treating the momentum is replaced by a Gaussian with dispersion $\Delta_p$,

$$\delta(\mathbf{p}) \longrightarrow \left(\frac{1}{2\pi\Delta_p^2}\right)^{3/2} \exp\left(-\frac{\mathbf{p}^2}{2\Delta_p^2}\right). \qquad (6)$$

Note that all coordinates are calculated in the c.m. system of the colliding nuclei. The relevant BUU input parameters are i) the number of test particles per nucleon (*i.e.* parallel runs or pseudo events, here chosen to 200), ii) nuclear charge and mass numbers of target and projectile, $A_t$, $Z_t$, $A_p$, $Z_p$, iii) the projectile energy $E_{\rm proj}$, iv) the impact parameter $b$, and v) the stiffness of the Equation of State (EoS), either hard ($\kappa = 380\,\mathrm{MeV}$), medium ($\kappa = 290\,\mathrm{MeV}$) or soft ($\kappa = 215\,\mathrm{MeV}$) [44]. A proton is considered "emitted" when the surrounding density falls below a value of $\rho_{\rm cutoff} = 0.02/\mathrm{fm}^3$ and when subsequent interaction with the mean field does not cause recapture into regions of higher density until the calculation is terminated at 150 fm/$c$. The cutoff value of about one eighth of normal nuclear matter density implies ceasing NN interactions in a sufficiently diluted nuclear matter. This choice was approved in systematic investigations of proton-proton correlations in $^{14}\mathrm{N} + {}^{27}\mathrm{Al}$ and $^{14}\mathrm{N} + {}^{197}\mathrm{Au}$ reactions at 75 $A\cdot$MeV [5], in $^{36}\mathrm{Ar} + {}^{45}\mathrm{Sc}$ collisions at 80 $A\cdot$MeV [11,14] and in $^{40}\mathrm{Ar} + {}^{197}\mathrm{Au}$ reactions at 200 $A\cdot$MeV [10].

Finally, for each run and each proton, the septuplet of space-time-momentum coordinates $N_i = (x, y, z, t, p_x, p_y, p_z)_i$ is taken from the BUU approach at the corresponding freeze-out time and then processed within the FSI model. The relevant parameters of the FSI model are the so-called "observation quantities", *i.e.* the sum momentum $P$, the momentum dispersion $\Delta_p$ and the polar angle $\theta^{\rm cm}$. These quantities are taken directly from the experimental distributions in the c.m. system, *e.g.*, $P = 2\,\langle p^{\rm cm}\rangle$. Typical values are $\theta^{\rm cm} = 45°$, $\Delta_p = 150$ MeV/$c$, and $\langle p^{\rm cm}\rangle = 300$ (400) MeV/$c$ for 400 (1500) $A\cdot$MeV beam energy.

### 3.1 System-size dependence

Figure 1 shows, for 400 $A\cdot$MeV beam energy, the system size dependence of the pp correlation function. Clearly, the pp correlation peak decreases with increasing system size and almost vanishes for the largest collision system Au + Au. The peaks (*i.e.* data within a relative-momentum range of $15 < q/\mathrm{MeV}/c < 50$) of the experimental correlation functions (symbols) are best described by the theoretical ones (lines) for apparent Gaussian radii of $R_0^* = (3.0 \pm 0.1)\,\mathrm{fm}$ for Ca + Ca, $(4.0 \pm 0.15)\,\mathrm{fm}$ for Ru + Ru and $(5.1 \pm 0.2)\,\mathrm{fm}$ for Au + Au collisions. Note that the term "apparent" means that neither the contribution of the finite emission duration (inappropriately called "lifetime", leading to an increase of the effective source radius) nor the effect of collective radial expansion of the participant zone (leading —via strong correlations of coordinate and momentum space— to a reduction of the effective source size) are taken into account [20]. In the following, the asterisk indicates apparent quantities, *e.g.* the sharp-sphere and r.m.s. radii $R^*_{\rm ss} = \sqrt{5}\,R_0^*$ and $R^*_{\rm rms} = \sqrt{3}\,R_0^*$, respectively. For Gaussian source distributions the effective radius can be written as [22]

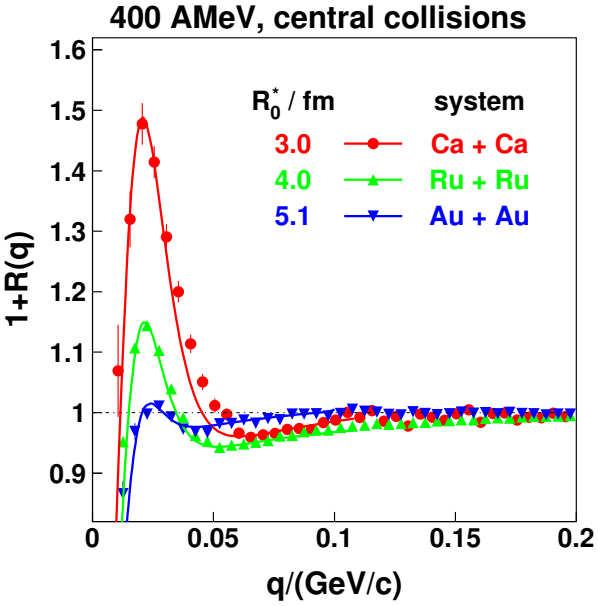


**Fig. 1.** Correlation functions of proton pairs from central collisions of Ca + Ca, Ru + Ru, and Au + Au at 400 $A\cdot$MeV. Experimental data (symbols) are compared to predictions of the FSI model with Gaussian sources and zero lifetime (lines). The corresponding apparent source radii are indicated.

$$R_0^* = \sqrt{\frac{R_0^2}{1+\epsilon} + (v\tau)^2}, \qquad (7)$$

where $\tau$ is the duration of emission, $v = P/2m$ is the pair velocity, and $\epsilon = \epsilon_{\rm flow}/\epsilon_{\rm therm}$ represents the ratio of radial flow energy $\epsilon_{\rm flow}$ and the energy of the random thermal motion $\epsilon_{\rm therm} = \frac{3}{2}T$.

For both the small- and the medium-size systems, our results can be compared directly with existing data: Gaussian radii $r_{\rm g}$ were derived from pp correlations measured with the "Plastic Ball" at BEVALAC for the reactions Ca + Ca and Nb + Nb, both at 400 MeV per nucleon, as function of proton multiplicity [9]. Taking into account the different radius definitions, *i.e.* $r_{\rm g} = \sqrt{2}R_0^*$, the apparent source radii for central collisions agree perfectly. Consequently, the freeze-out density of about 25% of normal nuclear matter density deduced in ref. [9] is in accordance with our results presented in sect. 3.2 below. Instead of disentangling the space-time-flow ambiguity of eq. (7) [20, 22], in the following we try to reproduce the experimental correlation functions by BUU+FSI model calculations.

Before we confront the data with theoretical correlation functions, we briefly focus onto the coordinate space distributions of freeze-out points from BUU calculations

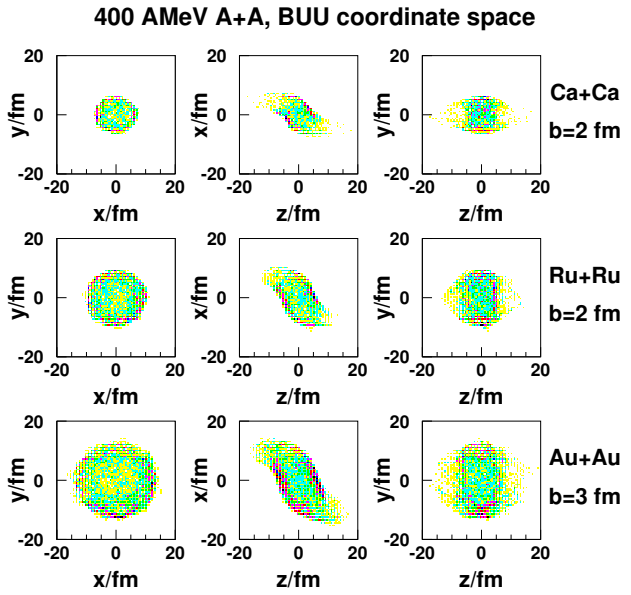


**Fig. 2.** Coordinate space distributions of freeze-out points of protons from central collisions of Ca + Ca (top), Ru + Ru (center), and Au + Au (bottom) at 400 $A \cdot$ MeV simulated by the BUU transport approach. The corresponding impact parameters are indicated at the right margin. The left, middle and right columns give the distributions in the $(y, x)$, $(x, z)$ and $(y, z)$ plane, respectively.

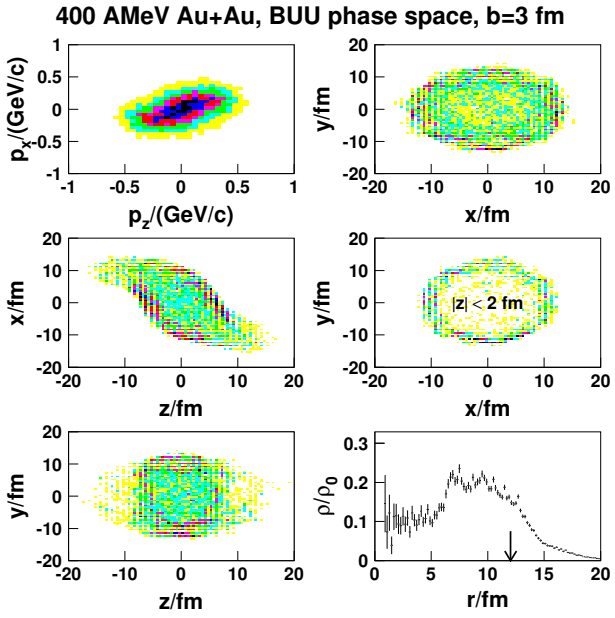


**Fig. 3.** Phase-space distribution of freeze-out points of protons from central collisions of Au + Au at 400 $A \cdot$ MeV simulated by the BUU transport approach for an impact parameter of $b = 3$ fm. Left column (from top to bottom): The distributions in the $(p_x, p_z)$, $(x, z)$, and $(y, z)$ plane. Right column: The $(y, x)$ distribution in total (top) and for a central $z$ slice, $|z| < 2$ fm (center). The bottom panel gives the corresponding radial density profile (in units of the saturation density). The arrow indicates the r.m.s. radius of the source.

displayed in fig. 2 for the three systems at 400 $A \cdot$ MeV beam energy. Note that the coordinates are not taken at fixed time but when the local density drops below the cut-off value. As expected, the proton source increases with increasing system size. Additionally to the coordinate space distribution shown in fig. 2, as an example for the Au + Au system, fig. 3 displays the momentum distribution projected onto the reaction plane $(p_x, p_z)$, the $(y, x)$ distribution for a central $z$ slice and the radial density profile. Here, the effective density is given in units of normal nuclear matter density, $\rho_0 = 0.168/\mathrm{fm}^3$. The corresponding r.m.s. radius $R_{\mathrm{rms}} = \sqrt{\langle r^2 \rangle}$ of the proton-emitting source is indicated by an arrow. No essential changes are observed from these phase-space plots when increasing the beam energy, except a trivial extension in momentum space. Since even the r.m.s. radius of the breakup configuration (cf. arrow in lower right panel) is almost the same for 400 and 1500 $A \cdot$ MeV beam energy, one would expect a very similar height of the pp correlation peaks. However, also the correlation of coordinate and momentum space, constituting a fast collective motion known as radial expansion, is expected to increase with beam energy. It should lead to a reduction of the apparent source radius and hence to an increase of the pp peak height (cf. eq. (7)). This presumption will be verified in sect. 3.2.

For 400 $A \cdot$ MeV beam energy, fig. 4 compares the experimental system-size dependence of the pp correlation function with the corresponding output of the BUU + FSI model. Hardly any differences have been found between

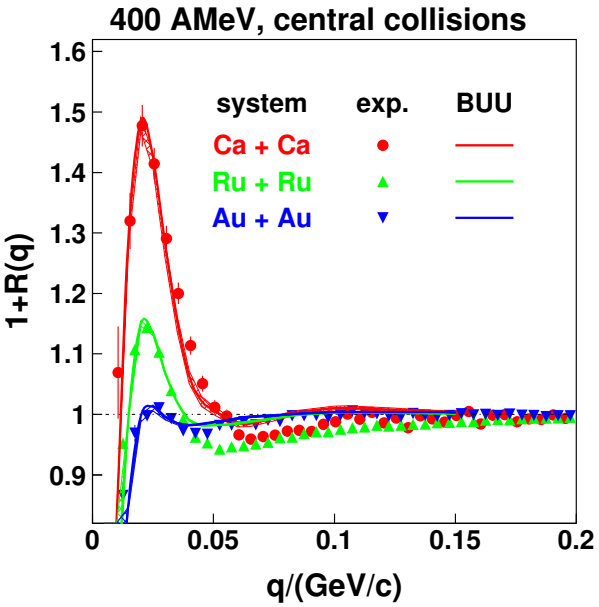


**Fig. 4.** The same as fig. 1, but here the experimental correlation functions (symbols) are compared to predictions of the BUU + FSI model (lines). The narrow hatched bands around the lines indicate the systematic variation of the calculations for the three different parameterizations of the EoS (see text).

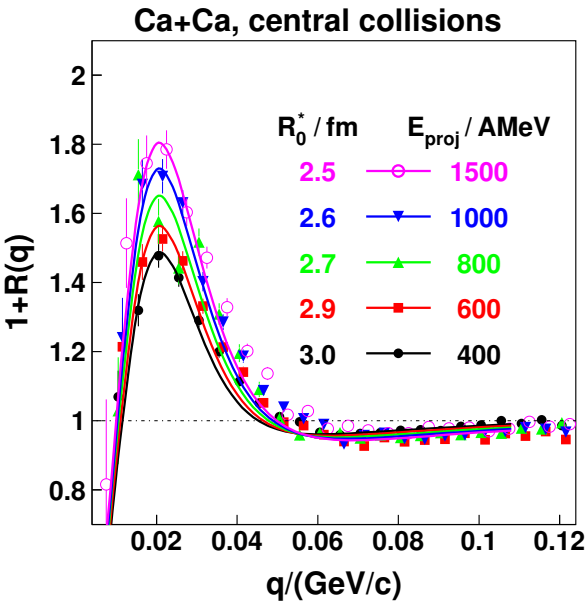


**Fig. 5.** Correlation functions of proton pairs from central collisions of Ca + Ca at projectile energies from 400 to 1500 $A \cdot$ MeV. Experimental data (symbols) are compared to predictions of the FSI model with Gaussian source and zero lifetime (lines). The corresponding apparent source radii are indicated.

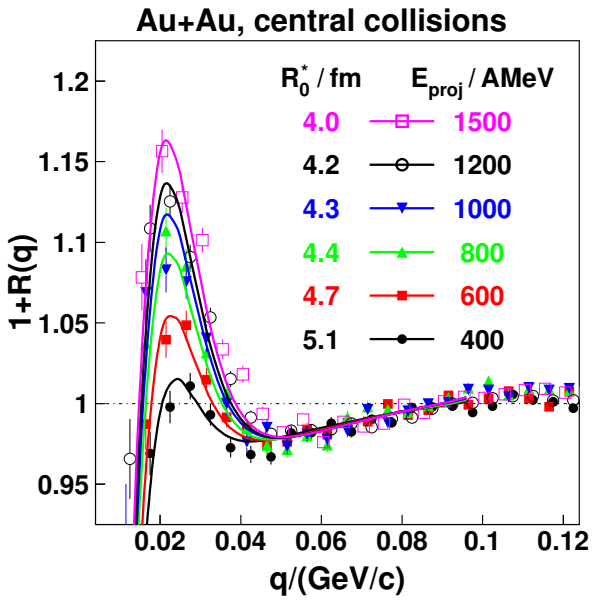


**Fig. 6.** Same as fig. 5, but for Au + Au collisions.

the pp correlation functions derived from BUU simulations using the three different parameterizations of the EoS, as can be inferred from the narrow hatched bands in fig. 4. (Similar findings have been reported for $^{14}$N + $^{27}$Al collisions at 75 $A \cdot$ MeV [5,8] and for $^{40}$Ar + $^{197}$Au reactions at 200 $A \cdot$ MeV [10].) Therefore, in the following we will restrict ourselves to the medium stiff EoS.

### 3.2 Beam energy dependence

Figure 5 shows the excitation function of experimental pp correlations from central collisions of Ca + Ca at beam energies from 400 to 1500 $A \cdot$MeV (symbols). A strong increase of the correlation peak is obvious corresponding to a decrease of the apparent source size. Indeed, when comparing with the theoretical correlation functions derived from the FSI model with static Gaussian sources and zero lifetime (lines), the experimental pp peak is best reproduced with apparent radii systematically decreasing from 3.0 fm at 400 $A \cdot$ MeV to 2.5 fm at 1500 $A \cdot$ MeV. This shrinking of the apparent source has to be traced back to two facts. First of all, at higher beam energies when the heavy-ion collisions is processing faster, the contribution of the emission duration onto the effective source radius is smaller. Usually, finite emission times imply a reduced Pauli suppression in emission direction and hence lead to an increase of the effective source radius [20]. Typically, for the energy range we are dealing with in the present investigation, these times are in the order of 10 fm/$c$ [20–22]. Secondly, also the collective (radial) expansion increases with increasing projectile energies. It is well known that strong correlations of coordinate and momentum space lead to a drastic reduction of the apparent source radius as derived from a comparison of the data with results of a FSI model incorporating the Koonin-Pratt formalism with static Gaussian sources and finite life (emission) times. 30% smaller radii are observed [20–22] for a ratio of collective to random thermal energies of unity [45].

Figure 6 shows the excitation function of experimental pp correlations from central collisions of Au + Au (symbols). From comparisons with the output of the FSI model (lines), we find an optimum reproduction of the experimental data in the peak region for apparent radii dropping from 5.1 fm at 400 $A \cdot$MeV to 4.0 fm at 1500 $A \cdot$MeV. The trend found in central Au + Au collisions is the same as for the smaller system Ca + Ca, but with lower peak values. This effect is expected due to the much larger number of involved nucleons in central Au + Au collisions. Looking at the volumes $V^* = 4\pi(R^*_{\rm ss})^3/3$ derived from the Gaussian radii given in figs. 1, 5 and 6, our expectations are confirmed: for the same beam energy, the volume ratio is approximately equal to the system size ratio of 197/40. Our investigation now points to the breakup densities derived from the given radii. With the given volumes and the number of participants estimated in sect. 2.1, apparent breakup densities (normalized to the density of normal nuclear matter) of $\rho^*/\rho_0 = (A_{\rm part}/V^*)/\rho_0 = 0.27 \pm 0.06$ ($0.29 \pm 0.05$, $0.29 \pm 0.05$) are deduced for Ca + Ca (Ru + Ru, Au + Au) collisions at 400 $A \cdot$MeV. These numbers increase to values of $0.47 \pm 0.11$ ($0.60 \pm 0.10$) for Ca + Ca (Au + Au) at beam energies of 1500 $A \cdot$ MeV. Here, the apparent breakup densities are not corrected for both the effects of collective radial expansion and finite duration of emission (cf. eq. (7)).

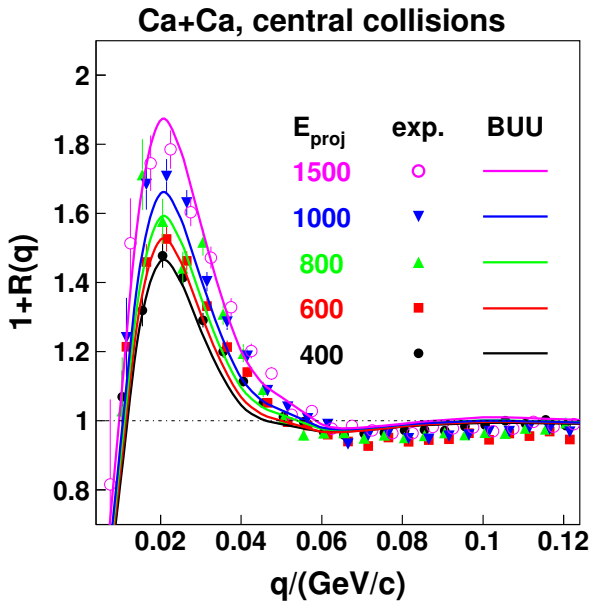


**Fig. 7.** Correlation functions of proton pairs from central collisions of Ca + Ca at projectile energies from 400 to 1500 $A\cdot$ MeV. Experimental data (symbols) are compared to predictions of the BUU+FSI model (lines).

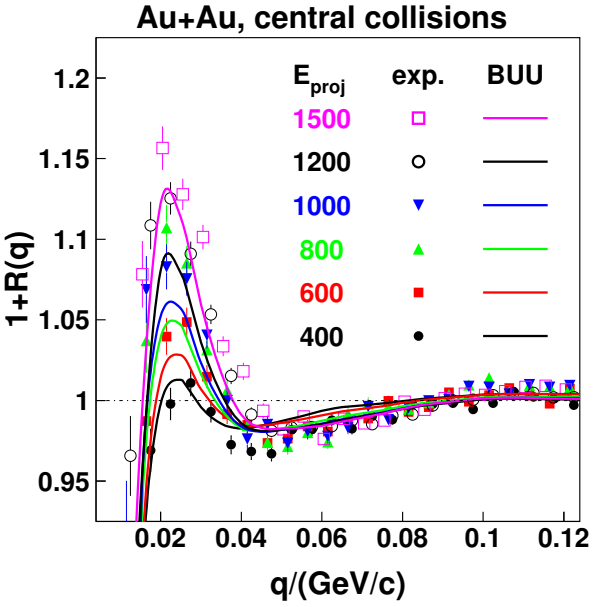


**Fig. 8.** Same as fig. 7, but for Au + Au collisions.

Finally, we confront the experimental beam energy dependence of two-proton correlations with the predictions of the BUU + FSI hybrid model. Figure 7 shows the excitation function of pp correlations for central Ca + Ca collisions in comparison to the model results. With the standard parameters in the transport approach the excitation functions are surprisingly well reproduced. Also for the larger system, Au + Au, the energy dependence is nicely described (cf. fig. 8). Here, the experimental pp correlation peaks are systematically slightly underestimated.

We want to point out that the agreement between our experimental correlation functions and those predicted by BUU is much better than in previous experiments performed at lower beam energies. Thus, pp correlation functions predicted by BUU calculations overestimated the measured central collision data of the reactions Ar + Au at 200 $A\cdot$MeV [10] and of Ar + Sc at 120 and 160 $A\cdot$MeV [16]. This deficiency of the BUU model was attributed to its inability to treat the population of particle unbound resonances and their decay via delayed particle emission [16, 28]. Obviously, at our higher beam energies this slow-emission component of the source function becomes unimportant, presumably since the number of heavy fragments drops strongly with energy [45]. Thus, the fast expansion-explosion scenario seems to be well modelled within the transport approach.

## 4 Summary

In the present paper, small-angle correlations of pairs of protons emitted in central heavy-ion collisions at beam energies from 400 to 1500 $A\cdot$MeV are investigated. New data are presented which substantially enlarge the experimental data basis on pp correlations in the SIS energy range.

The system size and beam energy dependences of the pp correlation peak are studied. The peak decreases, *i.e.* the apparent source radius increases, with increasing system size. This system size dependence is expected from the larger volume due to a larger number of participants in the central source. With increasing beam energy the peak of the pp correlation function increases, and hence the apparent source radius decreases. This behaviour is interpreted as the common action of shorter time scales and stronger collective radial expansion. Correlations of coordinate and momentum space constituting the latter radial flow are known to be responsible for the apparent shrinking of the source size found in small-angle correlation studies.

Both findings, shorter emission durations due to shorter time scales of the central heavy-ion collision and stronger radial expansion due to —increasing with pressure— space-momentum correlations, are well incorporated within microscopic transport models. Accordingly, using the Boltzmann-Uehling-Uhlenbeck transport approach, the phase-space points at freeze out are calculated and afterwards processed within a final-state-interaction model providing the two-proton correlation function. This BUU + FSI model well reproduces the system size and beam energy dependences of the experimental correlation function. However, the pp correlation function is found rather insensitive to the stiffness of the equation of state used in the transport model.

We are grateful for many discussions to H.W. Barz, B. Kämpfer and F. Dohrmann.

## References


1. S.E. Koonin, Phys. Lett. B **70**, 43 (1977).
2. S. Pratt, Phys. Rev. Lett. **53**, 1219 (1984); Phys. Rev. D **33**, 72, 1314 (1986); S. Pratt, M.B. Tsang, Phys. Rev. C **36**, 2390 (1987).
3. J. Pochodzalla, C.B. Chitwood, D.J. Fields, C.K. Gelbke, W.G. Lynch, M.B. Tsang, D.H. Boal, J.C. Shillcock, Phys. Lett. B **174**, 36 (1986).
4. P. Dupieux *et al.*, Phys. Lett. B **200**, 17 (1988); P. Dupieux *et al.*, Z. Phys. A **340**, 165 (1991).
5. W.G. Gong *et al.*, Phys. Rev. Lett. **65**, 2114 (1990); W.G. Gong *et al.*, Phys. Rev. C **43**, 781 (1991); W.G. Gong *et al.*, Phys. Rev. C **43**, 1804 (1991).
6. W. Bauer *et al.*, Phys. Rev. C **34**, 2127 (1986); W. Bauer, Nucl. Phys. A **471**, 604 (1987); W. Bauer, Phys. Rev. Lett. **61**, 2534 (1988); B.A. Li, W. Bauer, Phys. Lett. B **254**, 335 (1991); Phys. Rev. C **44**, 450 (1991); B.A. Li, W. Bauer, G.F. Bertsch, Phys. Rev. C **44**, 2095 (1991).
7. W. Bauer, C.K. Gelbke, S. Pratt, Annu. Rev. Nucl. Part. Sci. **42**, 77 (1992) and references cited therein.
8. W. Bauer, Nucl. Phys. A **545**, 369c (1992).
9. H.A. Gustafson, H.H. Gutbrod, B. Kolb, H. Löhner, B. Ludewigt, A.M. Poskanzer, T. Renner, H. Riedesel, H.G. Ritter, A. Warwick, F. Feik, H. Wieman, Phys. Rev. Lett. **53**, 544 (1984).
10. G.J. Kunde *et al.*, Phys. Rev. Lett. **70**, 2545 (1993).
11. M.A. Lisa *et al.*, Phys. Rev. Lett. **70**, 3709 (1993).
12. M.A. Lisa *et al.*, Phys. Rev. Lett. **71**, 2863 (1993).
13. M.A. Lisa *et al.*, Phys. Rev. C **49**, 2788 (1993).
14. D.O. Handzy *et al.*, Phys. Rev. C **50**, 858 (1994).
15. D.O. Handzy, S.J. Gaff, W. Bauer, F.C. Daffin, C.K. Gelbke, G.J. Kunde, Phys. Rev. C **51**, 2237 (1995).
16. D.O. Handzy *et al.*, Phys. Rev. Lett. **75**, 2916 (1995).
17. L. Martin, C.K. Gelbke, B. Erazmus, R. Lednicky, Nucl. Phys. A **604**, 69 (1996).
18. ALADiN Collaboration (S. Fritz *et al.*), Phys. Lett. B **461**, 315 (1999).
19. ALADiN Collaboration (C. Schwarz *et al.*), Nucl. Phys. A **681**, 279 (2001).
20. FOPI Collaboration (R. Kotte *et al.*), Z. Phys. A **359**, 47 (1997).
21. R. Kotte for the FOPI Collaboration, *Measuring the size of things in the universe: HBT interferometry and heavy ion physics*, in *Proceedings of CRIS'98, 2nd Catania Relativistic Ion Studies, Acicastello, Italy, June 8-12 1998* (World Scientific, Singapore, 1999) p. 299.
22. FOPI Collaboration (R. Kotte *et al.*), Eur. Phys. J. A **6**, 185 (1999).
23. D.A. Brown, P. Danielewicz, Phys. Lett. B **398**, 252 (1997).
24. D.A. Brown, P. Danielewicz, Phys. Rev. C **57**, 2474 (1998).
25. S.Y. Panitkin, D.A. Brown, Phys. Rev. C **61**, 021901 (2000).
26. D.A. Brown, S.Y. Panitkin, G. Bertsch, Phys. Rev. C **62**, 014904 (2000).
27. G. Verde, D.A. Brown, P. Danielewicz, C.K. Gelbke, W.G. Lynch, M.B. Tsang, Phys. Rev. C **65**, 054609 (2002).
28. G. Verde, P. Danielewicz, D.A. Brown, W.G. Lynch, C.K. Gelbke, M.B. Tsang, Phys. Rev. C **67**, 034606 (2003).
29. E895 Collaboration (P. Chung *et al.*), Phys. Rev. Lett. **91**, 162301 (2003).
30. D.A. Brown, F. Wang, P. Danielewicz, Phys. Lett. B **470**, 33 (1999).
31. S.A. Bass, C. Hartnack, H. Stöcker, W. Greiner, Phys. Rev. C **51**, 3343 (1995).
32. FOPI Collaboration (A. Andronic *et al.*), Phys. Rev. Lett. C **67**, 034907 (2003).
33. FOPI Collaboration (G. Stoicea *et al.*), Phys. Rev. Lett. **92**, 072303 (2004).
34. FOPI Collaboration (W. Reisdorf *et al.*), Phys. Rev. Lett. **92**, 232301 (2004).
35. FOPI Collaboration (W. Reisdorf *et al.*), Phys. Lett. B **595**, 118 (2004).
36. FOPI Collaboration (N. Bastid *et al.*), Nucl. Phys. A **742**, 29 (2004).
37. FOPI Collaboration (B. Hong *et al.*), Phys. Rev. Lett. C **66**, 034901 (2002).
38. FOPI Collaboration (A. Gobbi *et al.*), Nucl. Instrum. Methods A **324**, 156 (1993).
39. J. Ritman for the FOPI Collaboration, Nucl. Phys. Proc. Suppl. B **44**, 708 (1995).
40. Application Software Group, CN Division, CERN: GEANT3.21, CERN Program Library Long Writeup W5013 (1994).
41. FOPI Collaboration (B. Kämpfer *et al.*), Phys. Rev. C **48**, R955 (1993).
42. FOPI Collaboration (R. Kotte *et al.*), Phys. Rev. C **51**, 2686 (1995).
43. P. Danielewicz, G. Odyniec, Phys. Lett. B **157**, 146 (1985).
44. F. Daffin, K. Haglin, W. Bauer, Phys. Rev. C **54**, 1375 (1995).
45. FOPI Collaboration (W. Reisdorf *et al.*), Nucl. Phys. A **612**, 493 (1997).